

Editorial Manager(tm) for Solar Physics  
Manuscript Draft

Manuscript Number: SOLA276R2

Title: ANALYSIS OF SOLAR WIND EVENTS USING INTERPLANETARY SCINTILLATION (IPS) REMOTE SENSING 3D RECONSTRUCTIONS AND THEIR COMPARISON AT MARS

Article Type: Original Research

Section/Category:

Keywords: interplanetary scintillation; solar wind; mars solar wind pressure; solar wind 3D reconstruction

Corresponding Author: Dr B.V. Jackson,

Corresponding Author's Institution: University Of California

First Author: B.V. Jackson

Order of Authors: B.V. Jackson; Jason A Boyer; Pierre P Hick, Dr.; Andrew Buffington, Dr.; Mario M Bisi, Dr.; Dana H Crider, Dr.

Manuscript Region of Origin:

Abstract: Interplanetary Scintillation (IPS) allows observation of the inner heliospheric response to corotating solar structures and coronal mass ejections (CMEs) in scintillation level and velocity. With colleagues at STELab, Nagoya University, Japan, we have developed near real-time access of STELab IPS data for use in space-weather forecasting. We use a 3D reconstruction technique that obtains perspective views from solar corotating plasma and outward-flowing solar wind as observed from Earth by iteratively fitting a kinematic solar wind model to IPS observations. This 3D modeling technique permits reconstruction of the density and velocity structure of CMEs and other interplanetary transients at a relatively coarse resolution: A solar rotational cadence and 10° latitudinal and longitudinal resolution for the corotational model; and a one-day cadence and 20° latitudinal and longitudinal heliographic resolution for the time-dependent model. This technique is used to determine solar-wind pressure ("ram" pressure) at Mars. Results are compared with ram-pressure observations derived from Mars Global Surveyor magnetometer data (Crider, et al., 2003) for

the years 1999 through 2004. We identified 47 independent in situ pressure-pulse events above 3.5 nPa in the Surveyor data in this time period where sufficient IPS data were available. We detail the large pressure pulse observed at Mars in association with a CME that erupted from the Sun on 27 May 2003, which was a halo CME as viewed from Earth. We also detail the response of a series of west limb CME events, and compare their response observed at Mars about 160° west of the Sun-Earth line by the Global Surveyor with the response derived from the IPS 3D reconstructions.

Reviewer #1: I have only a single minor comment to the author:

Concerning your discussion and conclusions of the size of the peaks in line 24-30 at page 12: I still think that the argument is really being pushed to (or beyond) the limit of the observational evidence, in particular since the correlation is so poor. At the least I would strongly advice you to exchange line 28-30 "this slightly lower limit on the solar wind ram pressure SHOWS that these unaccounted for terms must be rather minor contributions" with "this slightly lower limit on the solar wind ram pressure INDICATES that these unaccounted for terms must be rather minor contributions".

A good wording change. The change has been made.

The editor's comments have also been included in this latest resubmission.

1  
2  
3  
4 **ANALYSIS OF SOLAR WIND EVENTS USING INTERPLANETARY**  
5 **SCINTILLATION (IPS) REMOTE SENSING 3D RECONSTRUCTIONS**  
6 **AND THEIR COMPARISON AT MARS**  
7  
8  
9

10 B. V. JACKSON<sup>1</sup>, J. A. BOYER<sup>1</sup>, P. P. HICK<sup>1</sup>, A. BUFFINGTON<sup>1</sup>,  
11 M. M. BISI<sup>1</sup>, AND D. H. CRIDER<sup>2</sup>

12 <sup>1</sup> *Center for Astrophysics and Space Sciences, University of California, San Diego, CA, 92093*  
13 *(E-Mail: byjackson@ucsd.edu)*

14 <sup>2</sup> *Catholic University of America, Washington, DC, 20064*  
15  
16  
17  
18

19 (Received 22 July 2006; accepted ??)  
20  
21  
22

23 **Abstract.** Interplanetary Scintillation (IPS) allows observation of the inner heliospheric  
24 response to corotating solar structures and coronal mass ejections (CMEs) in scintillation level  
25 and velocity. With colleagues at STELab, Nagoya University, Japan, we have developed near-  
26 real-time access of STELab IPS data for use in space-weather forecasting. We use a 3D  
27 reconstruction technique that obtains perspective views from solar corotating plasma and  
28 outward-flowing solar wind as observed from Earth by iteratively fitting a kinematic solar  
29 wind model to IPS observations. This 3D modeling technique permits reconstruction of the  
30 density and velocity structure of CMEs and other interplanetary transients at a relatively coarse  
31 resolution: A solar rotational cadence and 10° latitudinal and longitudinal resolution for the  
32 corotational model; and a one-day cadence and 20° latitudinal and longitudinal heliographic  
33 resolution for the time-dependent model. This technique is used to determine solar-wind  
34 pressure (“ram” pressure) at Mars. Results are compared with ram-pressure observations  
35 derived from *Mars Global Surveyor* magnetometer data (Crider, *et al.*, 2003) for the years  
36 1999 through 2004. We identified 47 independent *in situ* pressure-pulse events above 3.5 nPa  
37 in the *Mars Surveyor* data in this time period where sufficient IPS data were available. We  
38 detail the large pressure pulse observed at Mars in association with a CME that erupted from  
39 the Sun on 27 May 2003, which was a halo CME as viewed from Earth. We also detail the  
40 response of a series of west limb CME events, and compare their response observed at Mars  
41 about 160° west of the Sun-Earth line by the *Mars Global Surveyor* with the response derived  
42 from the IPS 3D reconstructions.  
43  
44  
45  
46  
47

## 48 1. Introduction

49

50 Interplanetary scintillation (IPS) observations of meter-wavelength intensity variations from  
51 point radio sources are one source of heliospheric remote-sensing information. These have  
52 long been used to measure small-scale (~200 km) density variations along the line-of-sight to a  
53 radio source (*e.g.*, Hewish, Scott, and Wills, 1964, Ananthakrishnan, Coles, and Kaufman,  
54 1980). IPS observations taken using the Cambridge IPS array in the UK (Houminer, 1971)  
55  
56  
57  
58  
59  
60  
61  
62  
63  
64  
65

1  
2  
3  
4 show structures that can be classified as either corotating or detached from the Sun (Gapper *et*  
5 *al.*, 1982; Hewish and Bravo, 1986; Behannon, Burlaga, and Hewish, 1991).

6 To optimize the use of IPS measurements and produce 3D global representations of the  
7 heliosphere from observations of point radio sources at specific locations in the sky covering a  
8 large range of elongations, we have developed a Computer Assisted Tomography (CAT)  
9 program (Jackson *et al.*, 1998; 2003; Jackson, Hick, and Buffington, 2002; Hick and Jackson,  
10 2003; Jackson and Hick, 2004) that fits these data to a solar-wind model. We fit STELab  
11 (Nagoya University) IPS observations (Kojima and Kakinuma, 1987; Jackson and Hick, 2004)  
12 and have operated a real-time forecasting system during the nine-month period each year when  
13 the STELab scintillation arrays take data. Two models are used. The first model assumes that  
14 the heliosphere is unchanging except for outward solar-wind flow over intervals of one solar  
15 rotation (a corotating model). In this model, solar rotation provides the primary change in  
16 perspective view for each observed location. The second model is time-dependent, allowing  
17 time to vary with an interval (usually one day) that is short compared with that of a solar  
18 rotation. This short interval imposes the restriction that the reconstructions primarily use  
19 outward solar-wind motion to give perspective views of each point in space. The results to  
20 date are commensurate with, but also limited by, the observational coverage, temporal and  
21 spatial resolution, and signal-to-noise available from the STELab data.

22 The *Mars Global Surveyor* magnetometer measurements of the Martian magnetosphere  
23 have provided a proxy for solar-wind dynamic pressure at Mars since 1997. For the period of  
24 this study from 1999 - 2004, no other instrument at Mars provided direct solar-wind density or  
25 velocity measurements. The *Mars Express* spacecraft, which arrived at Mars in 2004, although  
26 equipped with an Ion Mass Analyzer (IMA), does not *routinely* determine solar-wind  
27 parameters, and thus *Mars Global Surveyor* observations serve as an essential and more  
28 continuous measurement to characterize the interaction of the solar wind with Mars.

29 Previous 3D model reconstructions of velocities and densities at Earth (Jackson, Hick, and  
30 Buffington, 2002; Jackson and Hick, 2004) have shown good accuracy in retrospective  
31 analyses, and in forecasts. The present analysis extends this work to relative locations of the  
32 largest events observed at Mars. Here, STELab velocity and *g*-level (radio scintillation level  
33 relative to the nominal at that elongation) data are used to determine an arrival time and  
34 strengths of these pressure events. This analysis highlights the frontside halo CME event of 27  
35 May 2003, and a series of west limb CME events observed in September 2002, when Mars was  
36 opposite the Sun from Earth.

37 The next section describes the tomographic program developed to fit the IPS data and the  
38 technique used to deduce Mars ram pressure from the *Global Surveyor* magnetometer data.  
39 The third section compares amplitudes and timings of the tomographic model pressure peaks to  
40 the event peaks of larger than 3.5 nPa observed by the *Mars Global Surveyor*. The final  
41 section presents a summary and conclusions.

## 42 43 44 45 46 47 48 49 50 51 52 **2. 3D Reconstructions**

53 The present tomography technique reconstructs 3D corotating or time-dependent solar-wind  
54 velocity and density matrices by applying an inversion technique to the IPS data. In the solar  
55 corona, when structures do not evolve significantly (except for corotation) on a time scale of  
56 one solar rotation, rotation alone yields sufficient information for reconstruction of the quiet  
57  
58  
59  
60  
61  
62  
63  
64  
65

1  
2  
3  
4 corona. The corotational model, that assumes that observations to the east and to the west of  
5 the Sun are the same (see Jackson *et al.*, 1998), can be applied in this situation.

6 We also use a time-dependent 3D tomographic model. When a transient structure such as a  
7 heliospheric response to a CME is observed across a large range of solar elongations, it is  
8 viewed from widely different directions. This changing perspective is exploited to reconstruct  
9 a 3D time-dependent solar-wind model.

10 Both the corotating and time-dependent analyses incorporate the fact that line-of-sight  
11 observations are dominated by contributions from material closest to the Sun, because more  
12 scattering occurs there. However, no explicit assumptions are made about the distribution of  
13 velocity and density along these lines-of-sight. The inversion process begins with an assumed  
14 set of initial boundary conditions for the solar-wind model at 15 solar radii. In the case of the  
15 time-dependent model these boundaries are set at a regular time cadence (usually at one-day  
16 intervals centered at local noon in Nagoya, Japan). In the initial stage, these lower boundaries  
17 (source surfaces) are populated with an unstructured approximation of mass and velocity at that  
18 distance from the Sun. Currently, the model propagates mass and velocity outward from this  
19 source surface to beyond Earth using a purely kinematic model. The IPS observations are  
20 remotely sensed from as close to the Sun as  $11.5^\circ$  elongation and outward (the weak scattering  
21 regime at 327 MHz). Each line-of-sight is carried to as distant as two AU from Earth. The  
22 highest signal from the observations generally comes from the closest approach of the line-of-  
23 sight to the Sun, with that point being one AU in the solar direction and close to Earth beyond  
24 about  $60^\circ$  elongation. At the ends of the lines-of-sight, signals from solar-wind observations  
25 are less than 5% of the average total values. The 3D model is formed out to at least three AU  
26 from the Sun, well beyond the orbit of Mars. The model assumes outward radial flow and  
27 enforces conservation of mass and mass flux (Jackson *et al.*, 1998; Jackson and Hick, 2004).  
28 Given the initial velocities and densities on the inner boundaries, a fully 3D solar-wind model  
29 over time is propagated throughout the inner heliosphere.

30 Line-of-sight IPS scintillation levels and velocities are generated from the solar-wind  
31 reconstructions that correspond to the specified weighting function for the frequency of the IPS  
32 data used (for STELab observations this is 327 MHz). The differences between observed and  
33 modeled quantities are projected back onto the source surface, by tracing each solar-wind  
34 packet within the 3D model back to its origin on the source surface. The differences between  
35 the observed and model data are used to update the initial mass and velocity distribution on the  
36 source surface boundary (or boundaries in the case of the time-dependent reconstruction). The  
37 tomographic inversion takes place on the inner boundary by iteratively fitting the model to the  
38 observations until a least-squares minimum of observations to the model is obtained. When the  
39 model does not reproduce the solar wind at large solar distances accurately enough, the source  
40 surface values are altered to improve the fit. Convergence is assumed when differences no  
41 longer change by more than a few percent. This usually occurs well within the maximum  
42 allowed 18 iterations.

43 Since only a few thousand lines-of-sight exist in any one given solar rotation, the resolution  
44 is determined by a set of Gaussian filters having a  $10^\circ \times 10^\circ$  latitude and longitude resolution  
45 for the corotating model, and a  $20^\circ \times 20^\circ$  latitude and longitude resolution with a one-day  
46 temporal cadence for the time-dependent model. This resolution is good enough to determine  
47 the large-scale structure of solar-wind velocity and density. Tests show that after a few  
48 iterations, any specific residual of the initial boundary conditions is erased. The technique has  
49  
50  
51  
52  
53  
54  
55  
56  
57  
58  
59  
60  
61  
62  
63  
64  
65

1  
2  
3  
4 been used successfully to analyze corotating solar-wind structures (Jackson *et al.*, 1998) and  
5 CME-associated velocity and density structures using both IPS and Thomson-scattering  
6 observations (Jackson and Hick, 2004; Jackson *et al.*, 2006), and these compare favorably with  
7 other techniques used to invert the IPS data (Tokumaru *et al.*, 2005; 2006).  
8

9 Once the 3D solar-wind density and velocity have been calculated, time series at the  
10 position of Mars are extracted (interpolated in 3D in the case of the corotating model and in 4D  
11 in the case of the time-dependent model). A ram pressure ( $P$ ) is derived from these by the  
12 equation:  
13

$$14 \quad P = m n V^2 = 2 \times 10^{-6} n V^2. \quad (1)$$

15  
16  
17 The effective mass per electron ( $m$ ) is taken to be  $2.0 \times 10^{-24}$  g;  $P$  is in nPa,  $n$  is in electrons  
18  $\text{cm}^{-3}$ , and  $V$  is in  $\text{km s}^{-1}$ . Several assumptions determine the accuracy of this conversion. The  
19 density derived from the tomography is calibrated assuming a conversion from  $g$ -level small-  
20 scale electron-density fluctuations to density using a set of power-law relationships (Jackson *et*  
21 *al.*, 1998), in this case assumed to fit the Earth *in situ* proton density measurements from the  
22 ACE spacecraft for the density peak associated with the 14 July 2000 (Bastille Day) CME  
23 (Jackson *et al.*, 2003). As in this event, a background density of 5 electrons  $\text{cm}^{-3}$  at 1 AU was  
24 assumed. In addition, in the effective mass per electron ( $m$  above) assumes a 10% Helium  
25 abundance in the solar wind (Hildner *et al.*, 1975).  
26  
27

28 To compare the above values with *in situ* solar-wind measurements at Mars, the *Mars*  
29 *Global Surveyor* magnetometer measurements provide a proxy for solar-wind dynamic  
30 pressure at Mars by measuring the Martian magnetosphere magnetic-field magnitude  
31 (Vennerstrom *et al.*, 2003; Crider *et al.*, 2003). Since the Martian magnetosphere pressure only  
32 approximately balances the solar-wind dynamic pressure, it is important to find other ways to  
33 confirm these determinations at Mars.  
34  
35

36 Determination of the solar-wind ram pressure from the *Mars Global Surveyor* data is not  
37 entirely straightforward. First, magnetic-field measurements need to be selected distant from  
38 known Martian crustal sources of magnetic field. The technique further assumes that the  
39 contribution from Martian atmospheric gas pressure effects is small, and this includes thermal  
40 effects within the magnetic-pileup boundary. Magnetic pressure relative to the Martian surface  
41 is assumed to fall off relative to the angle of the incident solar-wind flow relative to the surface  
42 normal. Mapped during quiet times at Mars, these magnetic pressures form a curve fit to the  
43 location of the spacecraft relative to the solar zenith angle, and these relate to the pressure at  
44 the angle of incidence of solar-wind flow (Vennerstrom *et al.*, 2003). The analyses give good  
45 measurements of changes from one orbit pass to the next of the instrument through the pileup  
46 region of the Martian magnetosphere with an approximate time cadence of the orbital period of  
47 *Mars Global Surveyor*. Starting in March 1999, this period is a little under two hours. The  
48 period decreased from 44 hours to 2 hours from orbital insertion in September 1997 through  
49 March 1999. Absolute solar-wind pressures at Mars are derived from the knowledge of the  
50 magnetic-field pressure extrapolated to the stagnation point between the solar wind at the solar  
51 zenith even though the *Mars Global Surveyor* does not traverse this stagnation point.  
52 Consistency checks up to now have been provided by extrapolations from Earth to the vicinity  
53 of Mars over the period from 2 October 1997 to 31 December 1998 (Crider *et al.*, 2003) with  
54  
55  
56  
57  
58  
59  
60  
61  
62  
63  
64  
65

1  
2  
3  
4 additional checks at times of large events (e.g., Crider *et al.*, 2005). This proxy is consistent  
5 with those used by Verigin *et al.* (2004), who allow the obstacle shape to vary, and Brain *et al.*  
6 (2005), who include a variable gas pressure.  
7

### 8 9 **3. IPS Comparison with Mars Ram Pressure**

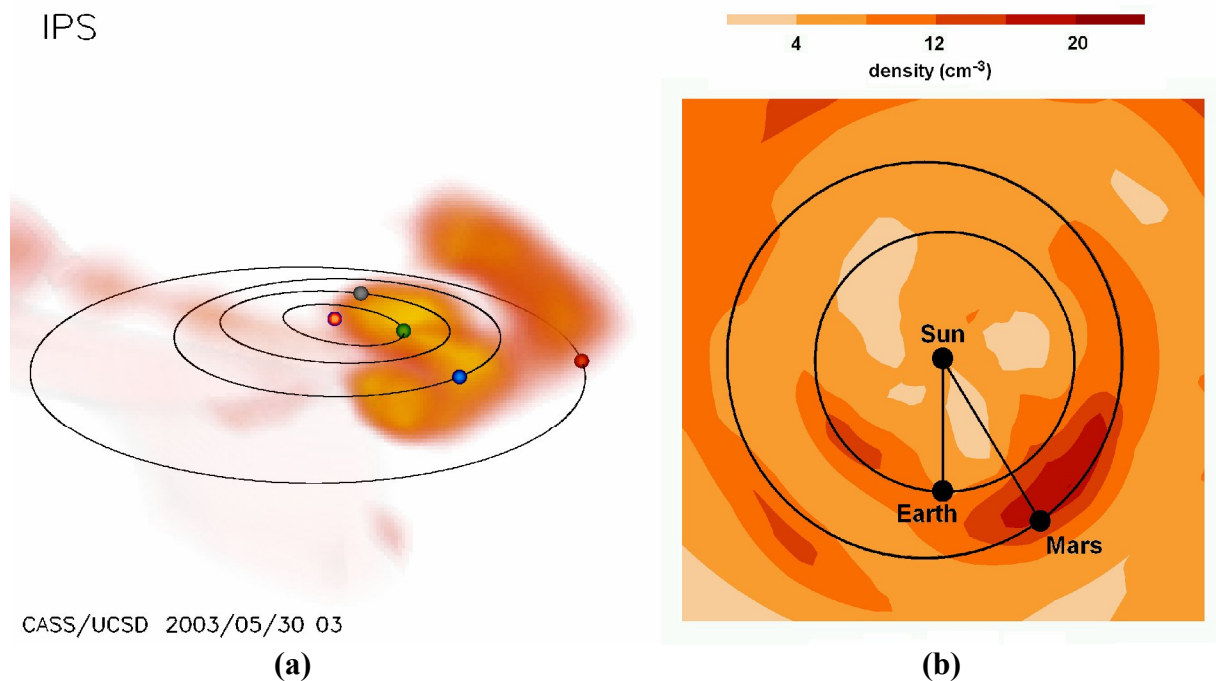
10  
11 We compare data gathered between 26 April 1999 and 7 December 2004, when both the  
12 STELab IPS arrays and *Mars Global Surveyor* were taking data. *Mars Global Surveyor* events  
13 above 3.5 nPa have pressures  $>1.5\sigma$  above the center of a Gaussian fit to the log of the solar-  
14 wind pressure. To compare with peaks in the IPS reconstructions smoothed by Gaussian filters  
15 both spatially and in time, the *Mars Global Surveyor* data were smoothed using a one-day  
16 “boxcar” filter, and then independent peaks of more than 3.5 nPa were selected to be compared  
17 with peaks in the IPS data. *Mars Surveyor* data were examined within  $\pm$ three days of the event  
18 peak time with the IPS data. In all, there were some 47 events above 3.5 nPa present in the  
19 *Mars Global Surveyor* data when the IPS arrays were operating, of which 20 were above 5 nPa  
20 and 5 were above 10 nPa. Of these 47 events, 42 were associated with peaks in the corotating  
21 analysis and 37 were associated with peaks in the time-dependent analysis. In order to  
22 determine whether an event on Mars was matched with an IPS event, several additional factors  
23 were considered including the event’s proximity to surrounding events, the shape and relative  
24 levels of the nearby IPS model peak values, and the relative value of the *Mars Surveyor* data  
25 peak above the local noise level.  
26  
27

28  
29 The very largest events observed in the *Mars Global Surveyor* analyses have obvious solar  
30 manifestations associated with CMEs, including the 2003 Halloween solar “superstorms”  
31 observed during the end of October and early November (Crider *et al.*, 2005). We have studied  
32 the 28 October 2003 event in detail using both the *Solar Mass Ejection Imager* (SMEI), (see  
33 Eyles *et al.*, 2003; Jackson *et al.*, 2005), and with 3D density reconstructions in conjunction  
34 with IPS velocity data (Jackson *et al.*, 2006). We include this event in this study because it  
35 shows a huge response in the IPS reconstruction and in the *Mars Surveyor* data with a peak that  
36 lags the IPS time-dependent 3D reconstruction peak by about one day. Even so, we note that  
37 this event is anomalous and worthy of a more lengthy discussion, because of its very high  
38 speed and solar-surface manifestations, and a response different in each spacecraft observing it  
39 near Earth. Otherwise, to characterize this study of many events throughout the time period of  
40 interest we have chosen several events observed at Mars: One is a “frontside” halo CME  
41 observed at the Sun on 27 May 2003, when Mars was in the hemisphere of the Sun toward  
42 Earth, and the others are a series of mostly west-limb CMEs observed in September 2002 when  
43 Mars was in the hemisphere away from Earth.  
44  
45

46  
47 A remote view of the IPS-derived density for the first event from the time-dependent model  
48 is shown in Figure 1a. This view shows the approximate shape of the density structure  
49 associated with this CME. Figure 1b shows the relative locations of Earth and Mars at the time  
50 of the CME event. Figure 2 compares the *Mars Surveyor* ram pressure time series with both  
51 the time-dependent and the corotating model. The halo CME of 27 May 2003, shows as a peak  
52 in the ram pressure beginning on 30 May 2003. The ram pressure peak in the *Mars Surveyor*  
53 analysis is one of the highest seen among the events with a value far above the minimum 3.5  
54 nPa threshold imposed here. The comparison with the time-dependent model (Figure 2b) is  
55  
56  
57  
58  
59  
60  
61  
62  
63  
64  
65

1  
2  
3  
4 observed well in the time-dependent 3D reconstructions, and perhaps is evident as a small  
5 delayed peak in the corotating analysis of Figure 2a.

6  
7 Figures 3 and 4 show the equivalent to Figures 1 and 2, but for the series of CMEs, the  
8 beginning of which reach Mars on about 16 September 2002. The peaks in the ram pressure  
9 for these events agree fairly well in the comparison with the time-dependent tomography  
10 analysis. This ram pressure event height reached a peak of about 3.8 nPa in the *Mars Surveyor*  
11 analysis at Mars, only slightly above the 3.5 value required for event comparison with the  
12 modeling. The only peak in the *Mars Surveyor* pressure analysis above the 3.5 nPa criterion  
13 during this interval occurred on 17 September 2002. As shown in the reconstruction, the major  
14 portion of the CME mass passed between the Earth and Mars. Although the peak shown in the  
15 modeling is not as clear or as dominant as in the frontside halo event of Figures 1 and 2, there  
16 is nonetheless a peak which also appears in the response shown in both the time-dependent and  
17 corotating models. Since the IPS observations go no closer to the Sun than 11.5° elongation,  
18 the derivation of IPS model ram pressure at Mars across the gap closer than this behind the Sun  
19 are determined from measurements made at locations on either side of it. This type of  
20 comparison was carried out for all of the original 47 *Mars Surveyor* ram pressure events above  
21 3.5 nPa, regardless of their position with respect to the Sun-Earth line.  
22  
23  
24  
25  
26



48  
49 **Figure 1. a)** Remote observer view of the reconstructed density for the halo CME event of 27  
50 May 2003. The view is from 30° above the ecliptic and about 30° east of the Sun-Earth line.  
51 Earth is the blue dot with its orbit shown as an ellipse beyond the orbits of Mercury and Venus.  
52 Mars is about to be engulfed by the CME. Electron density is scaled from 10 to 30  $e^- \text{ cm}^{-3}$  with  
53 an  $r^{-2}$  radial fall-off removed by the analysis. **b)** The relative locations of Earth and Mars at  
54 this time as seen from directly above the ecliptic plane, superimposed on the in-ecliptic density  
55 extracted from the tomographic reconstruction, also scaled as in a).  
56  
57  
58  
59  
60  
61  
62  
63  
64  
65

1  
2  
3  
4  
5  
6  
7  
8  
9  
10  
11  
12  
13  
14  
15  
16  
17  
18  
19  
20  
21  
22  
23  
24  
25  
26  
27  
28  
29  
30  
31  
32  
33  
34  
35  
36  
37  
38  
39  
40  
41  
42  
43  
44  
45  
46  
47  
48  
49  
50  
51  
52  
53  
54  
55  
56  
57  
58  
59  
60  
61  
62  
63  
64  
65

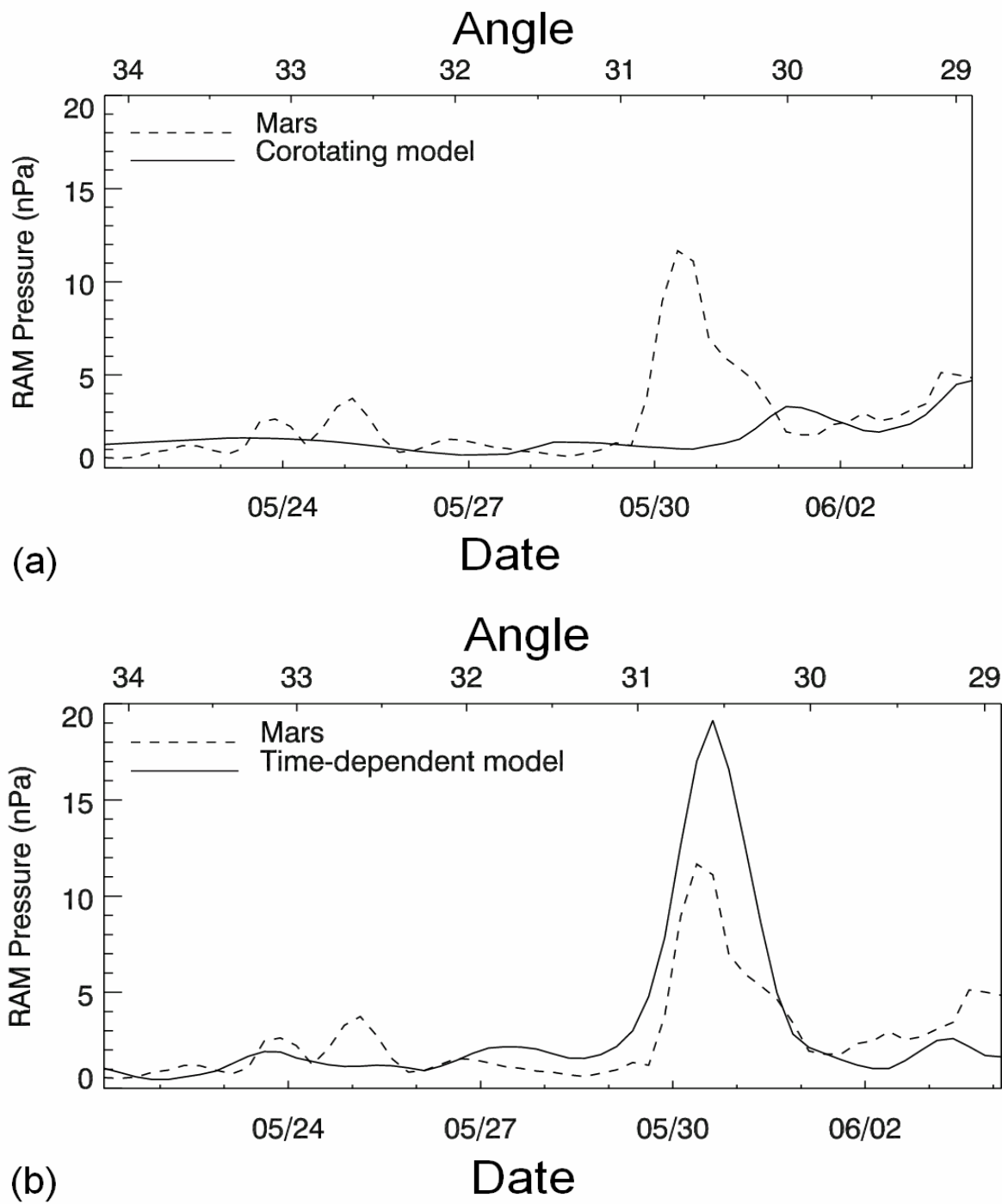
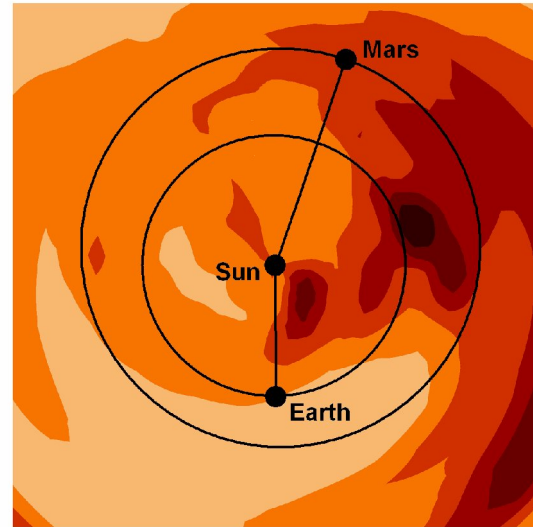
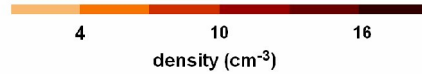
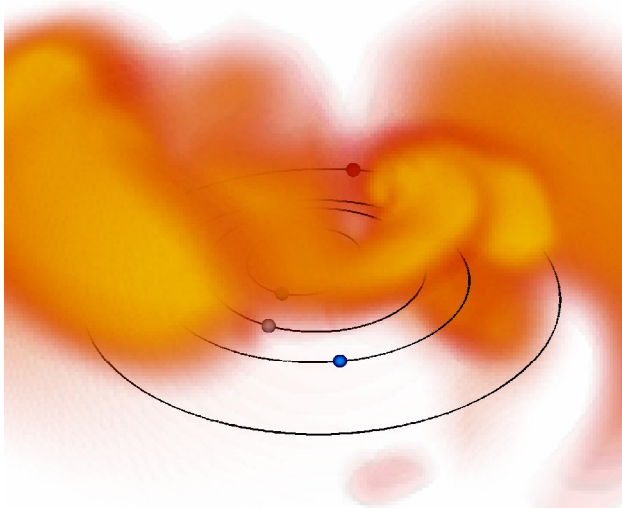


Figure 2. A comparison of IPS-derived ram pressure at Mars and *in situ* measurements derived from magnetic-field data for the time period from 21 May 2003 to 4 June 2003 covering the period of the 27 May 2003 CME event. The Mars *in situ* response to the event begins on 30 May 2003. The angle of Mars to the west of the Sun-Earth line is given at the top of each time series. **a)** Corotating model. **b)** Time-dependent model.

1  
2  
3  
4  
5  
6  
7  
8  
9  
10  
11  
12  
13  
14  
15  
16  
17  
18  
19  
20  
21  
22  
23  
24  
25  
26  
27  
28  
29  
30  
31  
32  
33  
34  
35  
36  
37  
38  
39  
40  
41  
42  
43  
44  
45  
46  
47  
48  
49  
50  
51  
52  
53  
54  
55  
56  
57  
58  
59  
60  
61  
62  
63  
64  
65

IPS



CASS/UCSD 2002/09/16 03

(a)

(b)

*Figure 3. a)* Remote observer view of the reconstructed density model associated with a series of west limb CME events as observed on 0300 UT 16 September 2002. Earlier CMEs to the solar northeast were also present. The view is from 30° above the ecliptic and about 5° to the east of the Sun-Earth line. Earth is shown as a blue dot on its orbit beyond the orbits of Mercury and Venus. Mars is shown as a dot on its orbit in the distance. Electron density is scaled from 5 to 15  $e^- \text{ cm}^{-3}$  with an  $r^{-2}$  radial fall-off removed by the analysis. The reconstruction shows that the primary portion of the CME dense material moves to the solar West as observed from the Earth with some of the material from these events present more than 180° from the Sun-Earth line. *b)* The relative locations of Earth and Mars at this time as seen from directly above the ecliptic plane superimposed on an ecliptic cut of density extracted from the tomographic reconstruction also scaled in density as in *a)*.

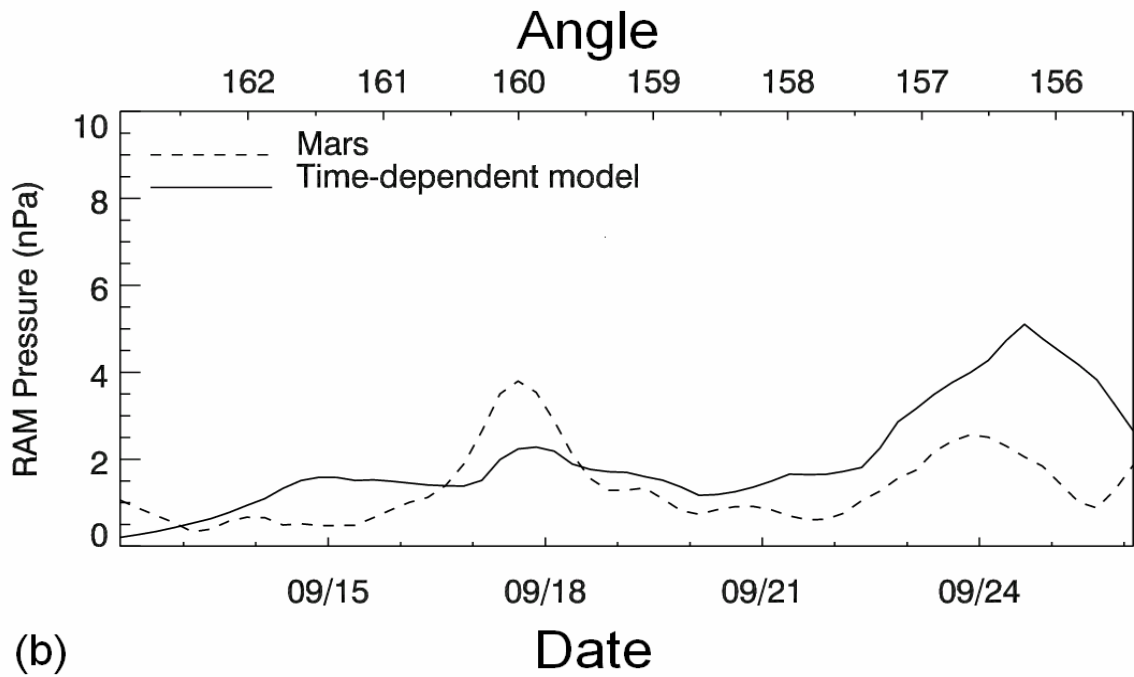
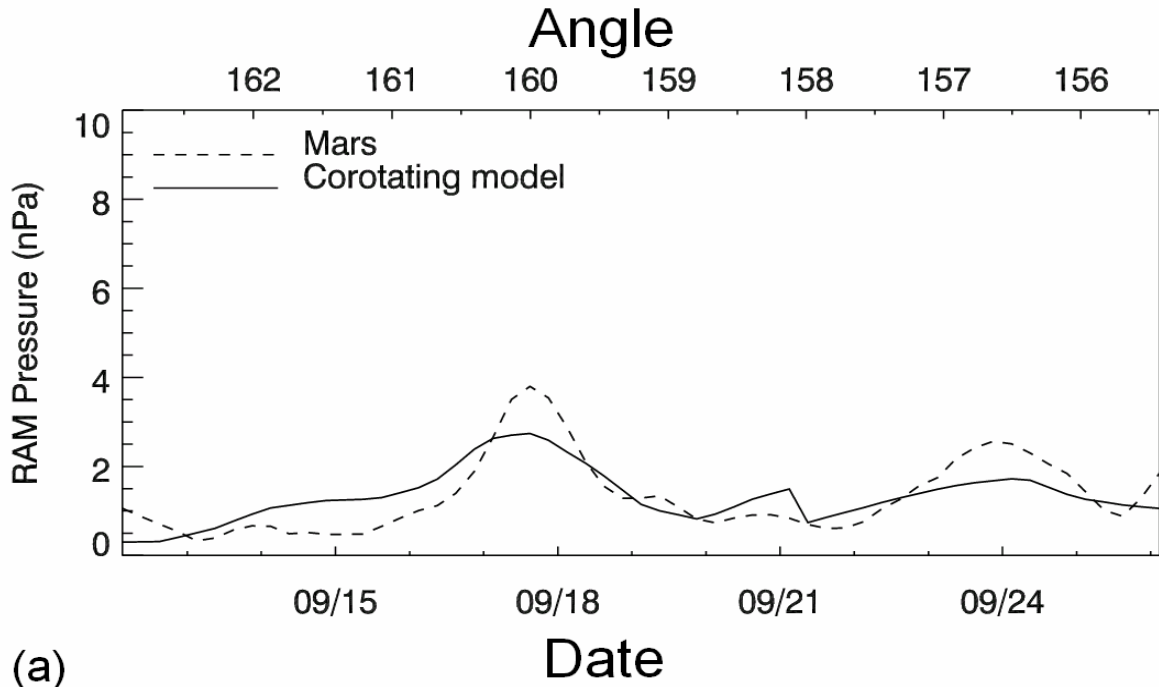
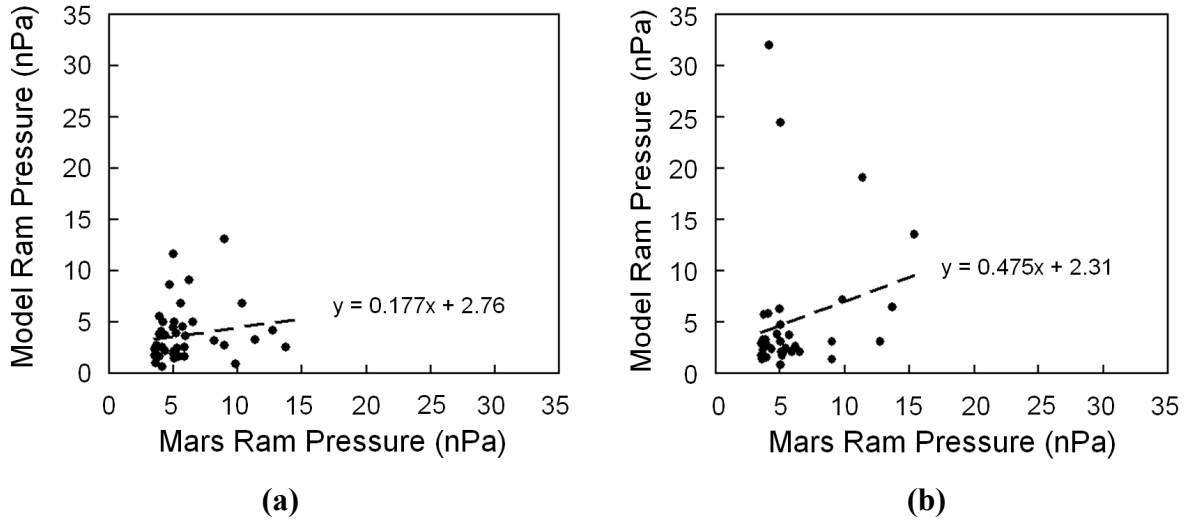


Figure 4. Mars time-series pressure analysis for the time period from 12 to 26 September 2002, associated with a series of CME events that occurred several days earlier. The Mars *in situ* response to the events begins about midway 15 September and continues for several days. The angle of Mars west of the Sun-Earth line is given at the top of each time series. The only peak in the *Mars Surveyor* pressure above the 3.5 nPa criterion within this time interval occurred on 17 September. **a)** Corotating model. **b)** Time-dependent model.

The ram pressure events observed by the *Mars Surveyor* are shown in a series of scatter plots and histograms detailing the amplitudes and correlation comparisons of these events with the 3D reconstructions from the IPS data. Figures 5a and 5b show the comparison in peak amplitude between the pressure events seen by the *Mars Surveyor* and the time-dependent and



**Figure 5.** Comparison between the ram pressure peak amplitude at Mars from the *Mars Surveyor* and the IPS reconstructions. **a)** 42 events are compared for the corotating model. **b)** 37 events are compared for the time-dependent model.

the corotating model, respectively.

Figures 6a to 6e show the results of comparing *Mars Surveyor* peak pressure time series values to IPS model peak values within three days of *Mars Surveyor* peak. The time shifts in peak values were determined for the most dominant peak within this three day period for both time series. These time lags were binned in one-day intervals, with negative shifts indicating that the IPS model peak values precede the peak in the *Mars Surveyor* ram pressure values. Conversely, positive shifts indicate the IPS model peak is late compared to the *Mars Surveyor* peak. Of the 47 dominant peaks in the *Mars Surveyor* data, only those events were retained where a peak existed within the three-day interval in the IPS pressure model value time series. The background level shown in each histogram was determined by finding the distance in time to the next nearest peak of more than 3.5 nPa in the *Mars Surveyor* analysis for each event, summing these times in days, and then dividing the number of events by this sum. In other words, with ten events having an average of ten days to the next event, the occurrence rate number would be 1.0.

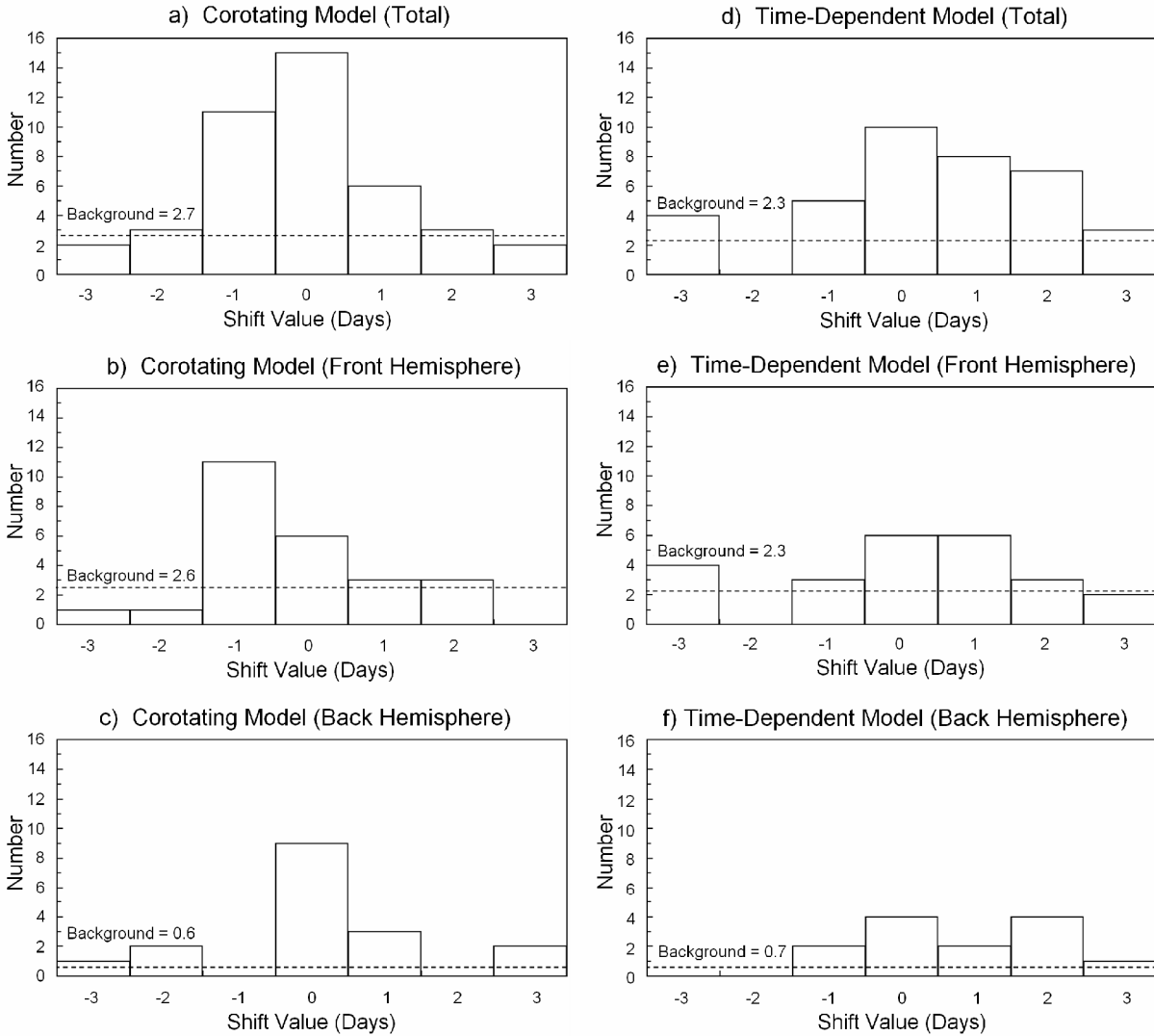


Figure 6. Histograms of the time lags between ram pressure peaks observed at Mars by the *Mars Global Surveyor* with the peaks observed in the corotating and time-dependent IPS models. A positive shift indicates a lag in the IPS model relative to the *Mars Global Surveyor* data, and a negative shift indicates a lead in the IPS model relative to the *Mars Global Surveyor* data. **a) – c)** give respectively the numbers of corotating total events, the Sun toward Earth events, and the Sun away from Earth events. **d) – f)** give respectively the numbers of time-dependent total events, the Sun toward Earth events, and the Sun away from Earth events.

#### 4. Summary and Conclusions

The 3D IPS solar-wind modeling clearly shows significant correlation in time with approximately the same amplitude when compared with the ram pressure events observed at Mars by the *Mars Global Surveyor*. This correlation persists even when Mars is in the hemisphere on the opposite side of the Sun from the Earth. The modeling combines two IPS data sets, namely the IPS velocity data and the IPS  $g$ -level data that are used as a proxy for bulk solar-wind density. We expected the 3D solar-wind reconstructions to give satisfactory solar-wind values at Mars on some occasions, given the numerous good comparisons of the model at Earth with *in situ* spacecraft observations of both density and velocity (see Jackson *et al.*, 1998; Jackson and Hick, 2004; Dunn *et al.*, 2005), but this tests the combination of these nearly separate IPS velocity and density analyses. In addition, it tests this at a location other than the one used for the remote-sensing observations.

However, the details of the comparisons at Mars have some interesting features. Amplitude comparisons for both time-dependent and corotating events (Figures 5a and b) show only a weak correlation. Most of the events in the study are just above the Mars ram pressure threshold of 3.5 nPa, with only a few events significantly above this relatively low threshold (a  $1.5\sigma$  measurement in the *Mars Global Surveyor* analyses). There is a tendency for the IPS modeling to give lower values for the event peaks. The average IPS model ram pressure value for the smaller peaks is just under 3 nPa for events just at the Mars event threshold of 3.5 nPa for both time-dependent and corotating models. Assuming that the associations of peaks in the *Mars Surveyor* analyses and the peaks in the IPS modeling analyses are accurate, this indicates that the IPS modeling gives ram pressures that are slightly lower (about 85%) than *Mars Surveyor*, *i.e.* the IPS modeling predicts a lower bulk density, or velocity, or both. Because the *Mars Global Surveyor* proxy does not account for all terms in the pressure balance, this slightly lower limit on the solar-wind ram pressure indicates that these unaccounted for terms must be rather minor contributions to the Mars magnetospheric solar-wind pressure.

The time-dependent 3D reconstruction is expected to primarily show transient events, and in the interval of study from 1999 - 2004, these are mostly CME-associated events. Although a time lag of zero days is the most frequent time lag for the time-dependent model, there are also time lags with a peak in the correlation above the noise level that are as distant as two days from the expected event time. In addition, there is a slight tendency for these time-dependent IPS-derived peaks to lag the *in situ* response seen by the *Mars Surveyor*. A two-day shift in the event time for the fastest CMEs is near the limit of what one would expect even though the model reconstructs a 3D structure that can miss Mars in both time and spatial dimensions, and that may not model CME deceleration accurately (see below). Clearly, the CME shape is not very accurately given since the IPS time-dependent model resolution is only  $20^\circ \times 20^\circ$  in latitude and longitude with a one-day temporal cadence, and the IPS measurements are obtained from sources that maximize their response at about 0.5 AU from the Sun (Jackson *et al.*, 1998). Regardless, CME events with speed near  $1000 \text{ km s}^{-1}$  should generally appear at Mars in the 3D reconstructions and in the *in situ* response seen by *Mars Surveyor* within one day of each other. We do not know the reason for this apparent slight discrepancy, if it is real. In speculation however, we note that there are often fast forward shocks that accompany fast CMEs and these often are associated with a large response at the Earth's magnetosphere. The IPS kinematic modeling assumptions contain no mechanism to produce a shock response in our

1  
2  
3  
4 analyses. From the Bastille-day CME (Jackson and Hick, 2004), and from other fast CME  
5 measurements where the modeled shock response is not well-observed in our analyses, we  
6 suppose that it is possible that the lag in the time-dependent model from the response at Mars  
7 could possibly be from an inadequate shock mechanism in our kinematic model. As a result,  
8 we would expect the IPS modeling to generally underestimate the propagation velocity of the  
9 CME and hence generally overestimate the CME response travel time from Sun to Mars. This  
10 may explain, in-part, the tendency for some IPS events at Mars to lag the *in situ* peak in the  
11 *Mars Surveyor* analyses. In addition, there are surely some event misidentifications in our  
12 sample. Often several CMEs leave the active Sun within days of each other, and these events  
13 may not appear as individual events at Mars nor can they be clearly separated in our current  
14 low-resolution time-dependent IPS modeling especially for the smaller events.

15  
16  
17 The corotating reconstruction shows primarily corotating solar features; with twice better  
18 spatial resolution in solar longitude to approximately a two-thirds day arrival discrepancy.  
19 However, during high periods of solar activity it is clearly a mistake to claim solar-wind  
20 features are corotating, especially in terms of density; clearly an ensemble of transient effects  
21 produces an average of features appearing to corotate from a given solar activity center. Thus,  
22 the histograms of Figure 6a - c in comparison with those of Figure 6d - f show that indeed  
23 regions of corotating high density and velocity during this period are at least partly made up of  
24 transient events, and that these extend in time over perhaps as many as several days.

25  
26  
27 We have presented results of the IPS 3D reconstruction techniques in a comparison with *in*  
28 *situ* solar-wind ram pressure analyses at Mars from the *Mars Global Surveyor*. As our models  
29 become more sophisticated, such as by using a 3D-MHD kernel in the tomographic analysis,  
30 we expect the comparisons to improve. In addition, we also expect to soon provide a similar  
31 result with the much higher resolution 3D reconstructions made possible using SMEI  
32 Thomson-scattering density modeling. This study does not specifically address the forecast  
33 capability of this technique as demonstrated with our near-real-time analyses of the IPS data.  
34 However, these same modeling techniques provide a forecast of solar-wind conditions at Mars  
35 when the IPS arrays are operating, and thus have the potential to provide a forecast of solar-  
36 wind conditions at Mars several days in advance. No spacecraft at Mars currently monitors  
37 solar-wind velocity and density regularly. When *in situ* solar-wind monitoring instruments are  
38 present on spacecraft near Mars, comparisons with the IPS and/or SMEI 3D reconstructions  
39 should become even more relevant and precise.

#### 40 41 42 43 44 **Acknowledgements**

45  
46 B.V. Jackson, J.A. Boyer, P.P. Hick, A. Buffington, and M.M. Bisi were supported at the  
47 University of California at San Diego by NSF grant ATM-0331513, and by NASA grants  
48 NAG5-13453, NNG05GM58G, and NAG5-11906; as well as AFOSR MURI grant SA3213  
49 subcontract to the University of California at Berkeley. D.H. Crider was supported at the  
50 Catholic University of America by NASA grants NAG5-11225 and NAG5-12235. The authors  
51 wish to acknowledge and thank the group at STELab, Nagoya University (M. Kojima, M.  
52 Tokumaru, K. Fujiki, and students) for their continued support, and for making IPS data sets  
53 available under the auspices of a joint collaborative agreement between the Center for  
54 Astrophysics and Space Sciences at UCSD and STELab.

## References

- Ananthakrishnan, S., Coles, W.A., and Kaufman, J.J., 1980, *J. Geophys. Res.*, **85**, 6025.
- Brain, D.A., Halekas, J.S., Lillis, R., Mitchell, D.L., Lin, R.P., and Crider, D.H., 2005, *Geophys. Res. Lett.* **32**, L18203, 10.1029/2005GL023126.
- Behannon, K.W., Burlaga, L.F., and Hewish, A., 1991, *J. Geophys. Res.*, **96**, 21, 213.
- Crider, D.H., Vignes, D., Krymskii, A.M., Breus, T.K., Ness, N.F., Mitchell, D.L., Slavin, J.A., and Acuña, M.H., 2003, *J. Geophys. Res.*, **108**, A12, 1461, doi:10.1029/2003JA009875.
- Crider, D.H., Espley, J., Brain, D.A., Mitchell, D.L., Connerney, J.E., Acuna, M.H., 2005, *J. Geophys. Res.*, **110**, A9, A09S21 10.1029/2004JA010881.
- Dunn, T., Jackson, B.V., Hick, P.P., Buffington, A., and Zhao, X.P., 2005, *Solar Phys.* **227**, 339.
- Eyles, C.J., Simnett, G.M., Cooke, M.P., Jackson, B.V., Buffington, A., Hick, P.P., Waltham, N.R., King, J.M., Anderson, P.A., and Holladay, P.E., 2003, *Solar Phys.*, **217**, 319.
- Gapper, G.R., Hewish, A., Purvis, A., and Duffett-Smith, P.J., 1982, *Nature* **296**, 633.
- Hewish, A. and Bravo, S., 1986, *Solar Phys.*, **106**, 185.
- Hewish, A., Scott, P.F., and Wills, D., 1964, *Nature*, **203**, 1214.
- Hick, P.P. and Jackson, B.V., 2003, *Proc. SPIE, San Diego*, 7-8 August 2003, **5171**, 287.
- Hildner, E., Gosling, J.T., MacQueen, R.M., Munro, R.H., Poland, A.I., and Ross, C.I., 1975, *Solar Phys.*, **42**, 163.
- Houminer, Z., 1971, *Nature Phys. Sci.*, **231**, 165.
- Jackson, B.V. and Hick, P.P., 2004, in *Solar and Space Weather Radiophysics Current Status and Future Developments*, D.G. Gary and C.U. Keller (eds.), *ASSL 314*, Kluwer, The Netherlands, 355.
- Jackson, B.V., Hick, P.L., Kojima, M., and Yokobe, A., 1998, *J. Geophys. Res.*, **103**, 12,049.
- Jackson, B.V., Hick, P.P., and Buffington, A., 2002, *Proc. SPIE, Waikoloa*, 22-28 August 2002, **4853**, 23.
- Jackson, B.V., Hick, P.P., Buffington, A., Kojima, M., Tokumaru, M., Fujiki, K., Ohmi, T., and Yamashita, M., 2003, in *Proc. Solar Wind X*, M. Velli, R. Bruno, and F. Malara (eds.), *AIP Conference Proc.* **679**, 75.
- Jackson, B.V., Buffington, A., Hick, P.P., Altrock, R.C., Figueroa, S., Holladay, P.E., Johnston, J.C., Kahler, S.W., Mozer, J.B., Price, S., Radick, R.R., Sagalyn, R., Sinclair, D., Simnett, G.M., Eyles, C.J., Cooke, M.P., Tappin, S.J., Kuchar, T., Mizumo, D., Webb, D.F., Anderson, P.A., Keil, S.L., Gold, R.E., and Waltham, N.R., 2005, *Solar Phys.* **225**, 177.
- Jackson, B.V., Buffington, A., Hick, P.P., Wang, X., and Webb, D., 2006, *J. Geophys. Res.*, **111**, A04S91, doi:10.1029/2004JA010942.
- Kojima, M. and Kakinuma, T., 1987, *J. Geophys. Res.*, **92**, 7269.
- Tokumaru, M., Kojima, M., Fujiki, K., Yamashita, M., and Jackson, B., 2005, presentation at the *XXVIIIth General Assembly of International Union of Radio Science (URSI)*, New Delhi, October 23-29.

1  
2  
3  
4  
5  
6  
7  
8  
9  
10  
11  
12  
13  
14  
15  
16  
17  
18  
19  
20  
21  
22  
23  
24  
25  
26  
27  
28  
29  
30  
31  
32  
33  
34  
35  
36  
37  
38  
39  
40  
41  
42  
43  
44  
45  
46  
47  
48  
49  
50  
51  
52  
53  
54  
55  
56  
57  
58  
59  
60  
61  
62  
63  
64  
65

Tokumaru, M., Kojima, M., Fujiki, K., Yamashita, M., and Jackson, B.V., 2006, *J. Geophys. Res.* (submitted).

Vennerstrom, S., Olsen, N., Purucker, M., Acuña, M. H., and Cain, J. C., 2003, *Geophys. Res. Lett.*, **30**, 1369, 10.1029/2003GL016883.

Verigin, M., Vignes, D., Crider, D., Slavin, J., Acuña, M., Kotova, G., and Remizov, A., 2004, *Adv. Space Res.*, **33**, 2222.